# Analytical Methods

Accepted Manuscript


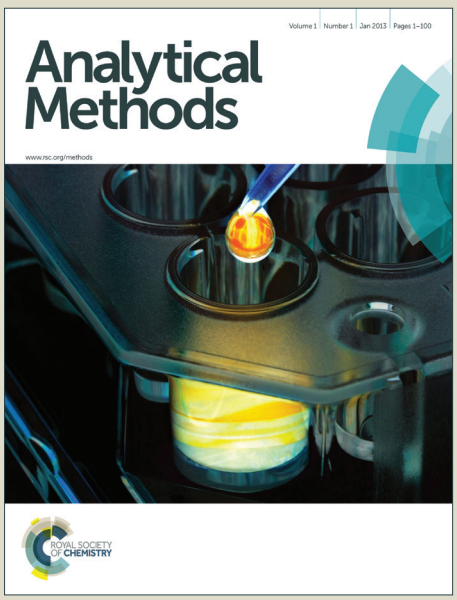





ROYAL SOCIETY OF CHEMISTRY

www.rsc.org/methods

## Graphical Abstract

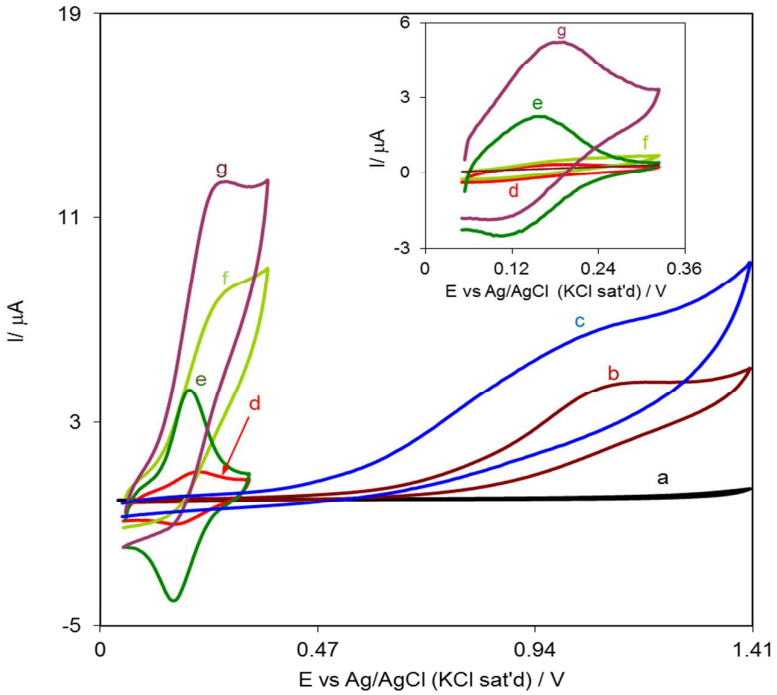

# Electrosynthesis and electrochemical characteristics of 2,2'-(4,5-dihydroxy-3-methoxy-1,2-phenylene)bis(3-oxo-3-phenylpropanenitrile): Application as a mediator for determination of hydroxylamine at a carbon nanotubes modified electrode surface

**Hamid R. Zare[a*], Milad Tashkili[a], Hossein Khoshro[a], Davood Nematollahi[b*], Ali Benvidi[a]**

[a]*Department of Chemistry, Yazd University, Yazd, 89195-741, Iran*

[b]*Faculty of Chemistry, Bu-Ali Sina University, Hamedan, Zip Code 65178-38683, Iran*

*Corresponding author: Tel.: +98 351 8122669: Fax: +98 351 8210991

*E-mail address:* hrzare@yazd.ac.ir (H.R. Zare)

**Abstract**

Electrosynthesis and electrochemical characteristics of an electrodeposited 2,2'-(4,5-dihydroxy-3-methoxy-1,2-phenylene)bis(3-oxo-3-phenylpropanenitrile), DMPP, film on multi-wall carbon nanotubes modified glassy carbon electrode (DMPP-MWCNT-GCE) and its role as a mediator for electrocatalytic oxidation of hydroxylamine are described. Cyclic voltammograms of the DMPP-MWCNT-GCE indicate a pair of well-defined and quasireversible redox couple with the surface confined characteristics at a wide pH range of 2.0-12.0. The charge transfer coefficient, α, and the charge transfer rate constant, $k_s$, of DMPP-MWCNT were calculated 0.51 and 10.7±1.7 $s^{-1}$, respectively. DMPP-MWCNT-GCE shows a dramatic increase in the peak current and a decrease in the overvoltage of hydroxylamine electrooxidation in comparison with that seen at a bare or MWCNT modified glassy carbon electrode. The kinetic parameters of electron transfer coefficient, α, the heterogeneous electron transfer rate constant, *k*', and the exchange current density, $j_0$, for oxidation of hydroxylamine at the modified electrode surface were determined using cyclic voltammetry. Differential pulse voltammetry (DPV) exhibits two linear dynamic ranges 1.0-10.0 μmol $L^{-1}$ and 10.0-300.0 μmol $L^{-1}$ as well as detection limit of 0.37 μmol $L^{-1}$ for hydroxylamine determination. Finally, the modified electrode was successfully used for determination of spiked hydroxylamine in a tap water sample.

*Keywords:* Electrosynthesis, Electrochemical behavior, Electrocatalytic oxidation, Catechol derivatives, Hydroxylamine determination

## 1. Introduction

Hydroxylamine, is an intermediate in two important microbial processes of the nitrogen cycle, being formed during nitrification and anaerobic ammonium oxidation.[1-3] Hydroxylamine is a natural product found in mammalian cells and bacteria. In the former, $NH_2OH$ may be formed from decomposition of nitrosothiols.[4] Hydroxylamine is a well-known mutagen, moderately toxic and harmful to human, animals, and even plants.[5,6] It is industrially used as pharmaceutical intermediates and in final drug synthesis, in nuclear fuel reprocessing, and in manufacturing semiconductors.[7-10] Thus, quantitative determination of hydroxylamine is also very important both in studies of biological processes and for industrial purposes.[11-14] The determination of hydroxylamine is usually executed by spectrophotometry,[15-20] gas or liquid chromatography with different detectors.[21-29] However, the processes involved in many of these methods are extremely complex, and the linear ranges are relatively narrow and have low precision. Among the different methods, electrochemical methods have several advantages over other methods such as simple, rapid, less time consuming and more selective and sensitive.[30] In electrochemical methods, various mediators have been used for hydroxylamine determination. For example, electrodes modified with mediators of nickel hexacyanoferrate-carbon ceramic,[31] an indenedione derivative,[32] coumestan derivative,[33] rutin,[34] alizarin red S,[35] ruthenium oxide nanoparticles,[36] chlorogenic acid,[37] and oracet blue,[38] have been earlier used for the determination of hydroxylamine. The modified electrodes have advantages and limitations. Therefore, it is of interest to have further efforts to fabricate certain modified electrodes that can improve the electrocatalytic characteristics and analytical parameters of hydroxylamine quantification. In this report, we examine the electrosynthesis of 2,2'-(4,5-dihydroxy-3-methoxy-1,2-phenylene) bis(3-

oxo-3-phenylpropanenitrile), DMPP, and its application as mediator for electrocatalytic determination of hydroxylamine. Our results indicate that DMPP multi-wall carbon nanotubes modified electrode offers some advantages including good stability, good repeatability, excellent reproducibility, high surface charge transfer rate constant, low detection limit and technical simplicity for electrocatalytic determination of hydroxylamine. Finally, to evaluate the utility of the modified electrode for analytical applications, it was used for voltammetric determination of hydroxylamine in water samples.

## 2. Experimental

### *2.1. Apparatus and chemicals*

All the electrochemical experiments, except electrosynthesis, were carried out using a potentiostat PGSTAT 101 model from AutoLab (Ecochemie, Netherlands), with Nova 1.7 software. Electrosynthesis experiments were performed by using a Sama-500 instrument potentiostat/galvanostat. A three electrode assembly was used for the experiments in a conventional electrochemical cell containing a glassy carbon electrode modified with multi-wall carbon nanotubes (MWCNT) and 2,2'-(4,5-dihydroxy-3-methoxy-1,2-phenylene)bis(3-oxo-3-phenylpropanenitrile) (DMPP), DMPP-MWCNT-GCE, as a working electrode, a graphite electrode as a counter electrode, and a Ag/AgCl/KCl (sat'd) as a reference electrode. Electrosynthesis was carried out using an assembly of four-graphite rods and a large stainless-steel gauze counter electrode (all electrodes from Azar Electrode Co., Iran). Reaction equipment of electrosynthesis was described in a previous paper.[39] pHs were measured with a Metrohm model 691 pH/mV meter.

3-Methoxycatechol and benzoylacetonitrile were prepared from Aldrich and Fluka. The multi-wall carbon nanotubes (10–20 nm in diameter, length of 5–20 μm, purity of 95%) were purchased from NanoLab Inc. (Brighton, MA). All others chemicals, purchased from Merck company, were of analytical reagent grades and were used without any further purification. The solutions were prepared just prior to use, and all the experiments were carried out at the ambient temperature of the laboratory (ca. 25°C). All the solutions were prepared with doubly distilled water. The buffer solutions (0.1 mol $L^{-1}$) were made up from $H_3PO_4$, and the pH was adjusted with 2.0 mol $L^{-1}$ of NaOH.

*2.2. Electrochemical synthesis of 2,2'-(4,5-dihydroxy-3-methoxy-1,2-phenylene)bis(3-oxo-3-phenylpropanenitrile), DMPP.*

A solution of phosphate buffer (80 mL; $c$ = 0.2 mol $L^{-1}$, pH 7.0) in water/acetonitrile (50/50 v/v) solution, containing 1.0 mmol of a 3-methoxycatechol (Scheme 1, **1**) and 1.0 mmol of benzoylacetonitrile (Scheme 1, **2**) was electrolyzed in an undivided cell at 0.25 V. The electrolysis was terminated when the current decreased by more than 95%. At the end of the electrolysis, the precipitated solid was collected by filtration and washed several times with water. The product was purified by column chromatography. The isolated yield of DMPP (Scheme 1, **5**) is 69%. M.p. 110-112 $^{o}$C. $IR_{(KBr)}$: 3429, 2930, 2365, 2206, 1699, 1653, 1593, 1521, 1448, 1362, 1372, 1220, 1095, 1005, 758, 692 $cm^{-1}$. $^{1}$H NMR (500 MHz DMSO-$d_6$): δ = 3.73 (s, 3H, methoxy), 4.76 (s, 1H), 6.34 (s, 1H), 6.38 (s, 1H), 7.49-7.94 (m, 10H), 8.64 (broad, 1H, OH), 9.29 (broad, 1H, OH). $^{13}$C NMR (125 MHz DMSO-$d_6$): δ = 30.9, 56.9, 62.2, 104.6, 110.3, 126.2, 129.7, 130.2, 130.5, 134.6, 135.1, 135.7, 146.9, 149.5. MS: m/z (relative intensity) = 399 [M-HCN] (20), 316 (90), 240 (21), 140 (40), 122 (39), 105 (100), 77 (22).

*2.3. Preparation and morphology of DMPP-MWCNT-GCE*

DMPP (1.0 mmol $L^{-1}$) was prepared from dissolving a 0.004 g DMPP in a few of acetonitrile and next the solution was diluted in a voltammetric cell to 10 mL of 0.1 M phosphate buffer (pH 7.0). To fabricate modified DMPP-GCE, the cleaned GCE was placed in above solution and the potential was scanned between -0.2 V and 0.8 V by twelve cycles at 25 mV $s^{-1}$. The preparation of MWCNT modified GCE (MWCNT-GCE) was performed by placing 1.0 µL of DMF-MWCNT suspension (1 mg/1 mL) on the cleaned GCE surface. Finally to prepare DMPP-MWCNT-GCE, MWCNT-GCE was placed in a 0.1 mol $L^{-1}$ phosphate buffer solution (pH 7.0) containing 1.0 mmol $L^{-1}$ of DMPP. It was modified with the same procedure that was described for DMPP-GCE.

Morphology of different electrodes was characterized using scanning electron microscopy. Fig. 3 shows the scanning electron micrographs (SEM) of bare GCE (Fig. 3A), MWCNT-GCE (Fig. 3B), and DMPP-MWCNT-GCE (Fig. 3C). The SEM of bare GCE (Fig. 3A) exhibits its own smooth surface. The distribution of MWCNT bundles is shown in Fig. 3B. Also, Fig. 3C displays that a thin film of DMPP has been adsorbed on MWCNT-GCE.

## 3. Results and discussion

*3.1. Electrochemical study of 3-methoxycatechol (**1**) in the presence of benzoylacetonitrile (**2**) for preparation of 2,2'-(4,5-dihydroxy-3-methoxy-1,2-phenylene)bis(3-oxo-3-phenylpropanenitrile), DMPP.*

Electrochemical oxidation of 3-methoxycatechol (**1**) was studied in the absence (Fig. 1, voltammogram (a)) and in the presence of benzoylacetonitrile (**2**) (Fig. 1, voltammogram (b)).

Voltammogram (a) , shows one anodic peak ($A_1$) and its cathodic peak ($C_1$), which correspond to the transformation of **1** to 3-methoxy-*o*-benzoquinone (**1ox**) and vice-versa (Scheme 1), through a quasi-reversible two-electron process. A comparison of voltammograms (a) and (b) indicates that in the presence of **2** the value of $I_{pC1}$ decreases. Also, in the second cycle of voltammogram (b), a new anodic peak ($A_0$) appears with an $E_p$ value of -0.10 V. The shift of the peaks $A_1$ and $C_1$ in the presence of **2** was due to the formation of a thin film of product at the surface of the electrode, inhibiting to a certain extent the performance of the electrode process.[40] Furthermore, with increasing the potential sweep rate, the peak current ratio ($I_{pC1}/I_{pA1}$) increases. An increase in the ratio of $I_{pC1}/I_{pA1}$ with increasing the scan rate for a mixture of **1** and **2** confirms the reactivity of **1ox** towards **2.** Cyclic voltammogram of benzoylacetonitrile (**2**) was recorded in the same condition (Fig. 1, voltammogram (c)). This voltammogram is established a totally irreversible electron-transfer process. Monitoring the electrolysis progress by linear sweep voltammetry synchronously during controlled-potential coulometry in $H_2O$ (0.2 mol $L^{-1}$ phosphate buffer, pH 7.0)/acetonoitrile (50/50 v/v) mixture containing **1** and **2** at 0.25 V shows that as the coulometry progresses, the $I_{pA1}$ decreases and $I_{pA0}$ increases. Peak $A_1$ disappears when the charge consumption becomes about $4e^-$ per molecule of **1**. Diagnostic criteria of cyclic voltammetry, the consumption of four electrons per molecule of **1** and the spectroscopic data of final product, support the structure of **5** (Scheme 1). According to our results, the Michael addition reaction of the anion **2An** to 3-methoxy-*p*-benzoquinone (**1ox**) leading to the intermediate **3** (Scheme 1). At the applied potential (0.25 V), this intermediate (**3**) is converted to *o*-benzoquinone **4**. In the final step, *o*-benzoquinone **4**, via a Michael reaction, is converted to the final product **5**.

*3.2. Electrochemical behavior of DMPP-MWCNT-GCE*

The electrochemical behavior of DMPP-MWCNT-GCE was characterized by cyclic voltammetry method. Fig. 2 shows cyclic voltammograms of the modified electrode, DMPP-MWCNT-GCE, in a 0.1 mol $L^{-1}$ phosphate buffer solution (pH 7.0) at different potential scan rates (5-130 mV $s^{-1}$). The plots of the anodic and cathodic peak currents ($I_p$) as a function of potential sweep rate are shown in Fig. 2, inset A. As it can be seen, the anodic and cathodic peak currents are proportional to the potential scan rate, suggesting that the redox process for DMPP-MWCNT-GCE has the characteristic of a surface-confined process. Insets B and C of Fig. 2 show the variations in the anodic and cathodic peak potentials ($E_{pa}$ and $E_{pc}$) as a function of the logarithm of the scan rate. Fig. 2, inset B, shows the peak-to-peak potential separation ($\Delta E_p = E_{pa} - E_{pc}$) is almost independent of the potential scan rate for scan rates below 200 mV $s^{-1}$. However, at higher scan rates, the separation between peak potentials increases with the increase of potential scan rates, indicating the limitation arising from the charge transfer kinetics. According to the theory given by Laviron,[41] if values of $n\Delta E_p > 200$ mV, the electron transfer coefficient ($\alpha$) and the surface electron transfer rate constant ($k_s$) can be determined from the slopes of the plots of Fig. 2, inset C. The graph $E_p = f(\log \nu)$ yields two straight lines with the slope $2.3RT/\alpha_a nF$ for the anodic peak and $-2.3RT/\alpha_c nF$ for the cathodic peak. Fig. 2, inset C, shows that the slopes of $E_{pa}$ and $E_{pc}$ versus log $\nu$ are 0.1232 and -0.1194, respectively. So, the estimated value for the kinetic parameters of $\alpha_a$ ($\alpha_a = 1-\alpha_c$) and $\alpha_c$ (anodic and cathodic transfer coefficients) are 0.48 and 0.5, respectively. We consider the average value of 0.51 for $\alpha_c$ ($\alpha$) and used in subsequent studies. The sum of transfer coefficients $\alpha_a$ and $\alpha_c$ minimally deviates from its normal value of 1. These results are in agreement with those reported for other deposited species.[42] Also, the

following equation can be used to estimate the electron transfer rate constant, $k_s$, between MWCNT-GCE and the DMPP:

$$\log k_s = \alpha\log(1-\alpha) + (1-\alpha)\log\alpha - \log(RT/nFv) - \alpha(1-\alpha)nF\Delta E_p/2.3RT \quad (1)$$

From the values of $\Delta E_p$ corresponding to the different potential scan rates of 900–5000 mV $s^{-1}$, the average value of $k_s$ was found to be 10.7 ± 1.7 $s^{-1}$ for pH 7.0.

*3.3. Effect of pH on the conditional formal potential of DMPP–MWCNT–GCE*

The voltammetric behavior of the DMPP–MWCNT–GCE was characterized at various pHs. Fig. 4 shows the cyclic voltammograms of the modified electrode in a 0.1 mol $L^{-1}$ phosphate buffer solution at the potential scan rate of 50 mV $s^{-1}$ at different pHs of 2.0–12.0. The inset of Fig. 4 shows with the increase of pH, the anodic and cathodic peak potentials are shifted toward less positive values. The redox reaction of the modified electrode can be written as follows:

$$\text{DMPP-MWCNT} \leftrightarrows \text{DMPP-MWCNT}_{(\text{oxidized form})} + mH^+ + 2e \quad (2)$$

The conditional formal potential, $E^{0\prime}$, is given by the following equation.[43]

$$E^{0\prime} = E^0 - (2.303mRT/2F)pH \quad (3)$$

where $E^0$ is the standard redox potential (or formal potential at pH=0); R, T and F are gas constant, temperature and Faraday constant, respectively. The inset of Fig. 4 shows that the plot's slope of $E^{0'}$ versus pH is −58.4 mV per unit of pH for pH range of 2.0 to 12.0. This slope is close to the Nernstian value of −59.2 mV corresponding to a two–electron, two–proton electrochemical reaction.

*3.4. Electrocatalytic oxidation of hydroxylamine at DMPP-MWCNT-GCE*

In order to test the electrocatalytic activity of DMPP film, the cyclic voltammograms at bare GCE, DMPP-GCE and DMPP-MWCNT-GCE were obtained in the absence and presence of 1.0 mmol $L^{-1}$ of hydroxylamine (Fig. 5). Voltammogram (a) of Fig. 5 shows the response of bare GCE in a 0.1 mol $L^{-1}$ phosphate buffer solution (pH 7.0) as the supporting electrolyte solution. Voltammograms (b) and (c) of Fig. 5 show the cyclic voltammograms of bare GCE and MWCNT-GCE in the presence of 1.0 mmol $L^{-1}$ of hydroxylamine, respectively. The cyclic voltammograms (d) and (e) are related to DMPP-GCE and DMPP-MWCNT-GCE in a 0.1 mol $L^{-1}$ phosphate buffer solution (pH 7.0). As it can be seen, there is a quasireversible redox couple for the both modified electrodes. Finally, voltammograms (f) and (g) were recorded under the same conditions with voltammograms (d) and (e), while the solution containing 1.0 mmol $L^{-1}$ of hydroxylamine. A comparison voltammograms of (e) and (g) as well as voltammograms (d) and (f) indicates that upon the addition of hydroxylamine, the anodic current increases markedly while the corresponding cathodic current disappears. Also, the cyclic voltammetric responses at DMPP-MWCNT-GCE (voltammograms (g)) and DMPP-GCE (voltammograms (f)) show a significant decrease in the overvoltage of hydroxylamine oxidation compared with that at MWCNT-GCE (voltammograms (c)). In addition, the current response the hydroxylamine electrocatalytic oxidation at DMPP-MWCNT-GCE (voltammograms (g)) is significant more than DMPP-GCE (voltammograms (f)). The electrocatalytic oxidation characteristics of hydroxylamine at various electrode surfaces at pH 7.0 are shown in Table 1. The results of Table 1 indicate that DMPP-MWCNT-GCE has the best electrocatalytic effect for hydroxylamine oxidation. It should be noted that use of MWCNT in the structure of the modified electrodes causes an increase in the effective surface area of the modified electrode and, hence, an increase in the current response of the analyte. On the other hand, DMPP as a mediator of the electron

transfer plays an effective role in decreasing the overpotential of hydroxylamine oxidation. Also, a comparison of the data in Table 1 indicates that a combination of MWCNT and DMPP improves the electrochemical characteristics of hydroxylamine oxidation. The electrocatalytic activity of 3-methoxycatechol (**1**) MWCNT-GCE for hydroxylamine oxidation was also investigated and the results have been shown in inset of Fig. 5. A comparison of voltammograms d, e, f, and g of this inset with voltammograms Fig. 5 indicates that the sensitivity of hydroxylamine quantitative determination is significantly decreased when 3-methoxycatechol was used as the electron transfer mediator instead DMPP.

The effect of potential scan rate on the electrocatalytic oxidation of hydroxylamine at DMPP-MWCNT-GCE was investigated by cyclic voltammetry. The scan rate dependence of cyclic voltammograms for DMPP-MWCNT-GCE in a 0.l mol $L^{-1}$ phosphate buffer solution (pH 7.0) containing 1.0 mmol $L^{-1}$ hydroxylamine is shown in Fig. 6. The inset A of Fig. 6 shows that a plot of the catalytic peak current versus the square root of the sweep rate is linear; suggesting that at sufficient overpotential the reaction is diffusion limited. The number of electrons participating in the oxidation process of hydroxylamine at the modified electrode surface, n, was obtained as n=2.04≅2.0. This value was calculated by using the slope of straight line of $I_p$ versus $v^{1/2}$ (Fig. 6, inset A) and according to the following equation which used for a totally irreversible diffusion-controlled process.[44]

$$\text{Slope} = 3.01 \times 10^5 n\,[(1-\alpha)n_\alpha]^{1/2} A C_b D^{1/2} \qquad (4)$$

where $(1 - \alpha)n_\alpha = 0.64$ (as obtained below from the Tafel plots), A, D and C are the electrode surface area ($cm^2$), diffusion coefficient ($cm^2\ s^{-1}$) and substrate concentration (mol $cm^{-3}$), respectively. Based on the above results, the electrocatalytic oxidation process of hydroxylamine

at the modified electrode surface can be described as an $E_qC_i$ catalytic ($E_qC'_i$) mechanism as shown in equations 5 and 6.

$$\text{DMPP-MWCNT} \rightleftharpoons \text{DMPP-MWCNT}_{(\text{oxidized form})} + 2H^+ + 2e \qquad (E_q) \qquad (5)$$

$$\text{DMPP-MWCNT}_{(\text{oxidized form})} + 2NH_2OH \xrightarrow{k'_h} \text{DMPP-MWCNT} + N_2O + H_2O \qquad (C'_i) \qquad (6)$$

The net catalytic oxidation of hydroxylamine at the modified electrode surface is given in the following equation.

$$2NH_2OH \longrightarrow N_2O + H_2O + 4H^+ + 4e \qquad (7)$$

For the case of slow potential scan rates, $v$, and large catalytic rate constant, $k'_h$, Andrieux and Saveant,[45] developed a theoretical model for a heterogeneous catalytic reaction:

$$I_{cat} = 0.496nFAC_b v^{1/2}(nFD/RT)^{1/2} \qquad (8)$$

where D and $C_b$ are the diffusion coefficient ($cm^2\ s^{-1}$) and the bulk concentration (mol $cm^{-3}$) of the substrate (hydroxylamine in this case), respectively. Low values of $k'_h$ result in coefficient values lower than 0.496. For low potential scan rates (2–24 mV $s^{-1}$), the average value of this constant was found to be 0.29 for DMPP-MWCNT-GCE with a net surface area, A, of 0.0314 $cm^2$, and D= $2.42\times10^{-6}$ $cm^2\ s^{-1}$ (obtained by chronoamperometry as below) in the presence 1.0 mmol $L^{-1}$ of hydroxylamine. According to the approach of Andrieux and Saveant,[45] and using the data of Fig. 1 in their theoretical paper,[45] an average value of $k'_h$ was calculated as $(1.35\pm0.48)\times10^{-3}$ cm $s^{-1}$. In addition, the plot of the scan rate-normalized current ($I\ v^{-1/2}$) versus the potential scan rate (Fig. 6, inset B) supports an $E_qC'_i$ mechanism for electrooxidation of hydroxylamine. In order to obtain information on the rate-determining step, the Tafel plots were drawn using the data from the rising part of the cyclic voltammograms (known as Tafel region) recorded at different potential scan rates 6-12 mV $s^{-1}$ (Fig. 6, inset C). This part of the voltammogram was affected by the electron transfer kinetics between hydroxylamine and

DMPP-MWCNT-GCE. These data can be used to evaluate the kinetic parameters of hydroxylamine electrocatalytic oxidation at the modified electrode surface. Referring to Eq. 6 the charge transfer coefficient, α, of the electrode process can be evaluated from the slope of the anodic Tafel plot, if the rate-determining step of the electrode process includes a one-electron transfer, $n_\alpha$=1,[43]

$$\text{Anodic Tafel slope} = (1-\alpha)n_\alpha F/2.3RT \quad (9)$$

Based on the above results and considering the slopes of the Tafel plots in Fig. 6, inset C, the average anodic charge transfer coefficient, $\alpha_{ave}$, is evaluated as 0.36±0.02. Also, the exchange current density, $j_0$, is obviously readily accessible from the intercept of the Tafel plots,[43] The average value of the exchange current density, $j_0$, of hydroxylamine at the DMPP-MWCNT-GCE surface is found to be 1.14±0.17 μA $cm^{-2}$.

*3.5. Chronoamperometric studies*

Chronoamperometry technique was employed for the determination of diffusion coefficient of hydroxylamine. For an electroactive material with a diffusion coefficient D, the current response under diffusion control has been described by Cottrell's equation.[43]

$$I = nFAD^{1/2}C_b\pi^{-1/2}t^{-1/2} \quad (10)$$

where D, $C_b$ and A are the diffusion coefficient ($cm^2$ $s^{-1}$), bulk concentration (mol $cm^{-3}$) of hydroxylamine and the electrode surface area, respectively. Chronoamperograms were obtained by setting the working electrode potential at 220 mV for various concentrations of hydroxylamine (Fig. 7). The inset A of Fig. 7 shows the experimental plots of I versus $t^{-1/2}$ with the best fits for different concentrations of hydroxylamine employed. The slopes of the resulting straight lines were then plotted versus the hydroxylamine concentration (inset B of Fig. 7), from

whose slope and using the Cottrell equation,[43] calculated a diffusion coefficient of $2.42\times10^{-6}$ $cm^2$ $s^{-1}$ for hydroxylamine. Although the obtained value of the diffusion coefficient is in good agreement with the values reported by others,[35,46] it is higher than those reported in Refs.[32,37,47]

*3.6. Differential pulse voltammetric determination of hydroxylamine at the DMPP-MWCNT-GCE surface*

Since differential pulse voltammetry, DPV, has a much higher current sensitivity than cyclic voltammetry, it was used to estimate the detection limit and also determination of hydroxylamine in different synthetic and real samples. The effects of increasing the concentration of hydroxylamine on the voltammograms are presented in Fig. 8. Also, insets A and B of Fig. 8 clearly show that the plot of the peak current versus the hydroxylamine concentration is constituted of two linear segments with different slopes 0.1088 μA $\mu mol^{-1}$ L and 0.0126 μA $\mu mol^{-1}$ L, corresponding to two different ranges of 1.0-10.0 μmol $L^{-1}$ and 10.0-300.0 μmol $L^{-1}$. A comparison of the sensitivities of the two linear segments indicates a decrease of the sensitivity in the second linear range of the calibration plot. It is well known that when an analyte concentration increases in a solution, follow up thickness of the diffusion layer and the mass transfer limitation are reduced.[43] Thus, it is logical to conclude that, under these conditions, the electron transfer kinetic between hydroxylamine and the modifier has a main role for the current limitation. In other words, a decrease in the sensitivity of the calibration plot as well as the relative independence of the peak current of the analyte concentration in high analyte concentrations are likely to be due to the electron transfer kinetic limitation between hydroxylamine and the modifier.

According to the method mentioned in the literature,[48] the lower detection limit $C_m$ was obtained using the equation (11).

$$C_m = 3s_{bl}/m \quad (11)$$

In above equation $s_{bl}$ is the standard deviation of the blank response (μA) and m is the slope of the calibration plot in the first linear range. From the analysis of resulting data, the detection limit of 0.37 μmol $L^{-1}$ was estimated for hydroxylamine determination using the modified electrode. The dynamic range and the detection limit of the recently reported modified electrodes are shown in Table 2.[14,31-38,47,49-60] As it can be seen, the capabilities of the proposed sensor are superior in most cases than the others. Using the modified electrode, the relative standard deviation (RSD) corresponding to 10 replicate measurements of 100.0 μmol/L hydroxylamine was 1.1%. These data indicate that the modified electrode is stable and also the results obtained at the DMPP-MWCNT-GCE surface are reproducible and does not undergo surface fouling during voltammetric measurements.

*3.7. Application of* DMPP-MWCNT-GCE *for determination and recovery of hydroxylamine in real samples*

To confirm the usefulness of DMPP-MWCNT-GCE, the applicability and reliability of the proposed modified electrode were tested for the hydroxylamine determination in real samples. In this experiment tap water samples was analyzed using the above technique. For this purpose 5.0 mL of the water sample was diluted to 10.0 mL with 0.1 mol $L^{-1}$ phosphate buffer solution (pH 7.0). Then, the water sample was spiked with 50.0 μL and 100.0 μL of 10.0 mmol $L^{-1}$ hydroxylamine solution and their recovery was determined by differential pulse voltammetry measurements at the DMPP-MWCNT-GCE surface and utilizing a calibration plot which are

shown in Fig. 8. Based on the currents of repeated voltammograms (n = 4), the hydroxylamine concentrations in the spiked tap water sample were calculated as reported in Table 3. The results in Table 3 show that the relative standard deviations (RSD%) and the recovery rates of the spiked hydroxylamine are acceptable.

## 4. Conclusions

This study demonstrate electrosynthesis and electrocatalytic activity of 2,2'-(4,5-dihydroxy-3-methoxy-1,2-phenylene)bis(3-oxo-3-phenylpropanenitrile), DMPP, for hydroxylamine determination. The kinetic parameters of the electron transfer rate constant, $k_s$, and the transfer coefficient, α, corresponding to the redox reaction of DMPP deposited on MWCNT-GCE were estimated. The results show that the characteristics of electrocatalytic oxidation of hydroxylamine are significantly improved at the DMPP-MWCNT-GCE surface in comparison with a bare or MWCNT glassy carbon electrode. The heterogeneous catalytic electron transfer rate constant, $k'_h$, and the transfer coefficient, α, were also determined for the oxidation of hydroxylamine at the modified electrode surface using a cyclic voltammetry method. The diffusion coefficient of hydroxylamine was calculated as $2.42\times10^{-6}$ $cm^2$ $s^{-1}$ under experimental conditions, using chronoamperometric results. Differential pulse voltammetric (DPV) measurements exhibit two linear ranges of 1.0–10.0 μmol $L^{-1}$ and 10.0–300.0 μmol $L^{-1}$ and a detection limit of 0.37 μmol $L^{-1}$ for hydroxylamine. Finally, the proposed modified electrode was successfully applied to determine hydroxylamine in a tap water sample. Low detection limit, excellent catalytic activity, good repeatability for hydroxylamine determination, simplicity of

preparation, good reproducibility, and low cost of the modified electrode are the important advantages of DMPP-MWCNT-GCE.

## References


1 D. J. Arp and L. Y. Stein, *Crit. Rev. Biochem. Mol. Biol.*, 2003, **38**, 471-495.

2 M. S. Jetten, *Plant and Soil*, 2001, **230**, 9-19.

3 T. Hofman and H. Lees, *Biochem. J*, 1953, **54**, 579.

4 P. S. Y. Wong, J. Hyun, J. M. Fukuto, F. N. Shirota, E. G. DeMaster, D. W. Shoeman and H. T. Nagasawa, *Biochemistry*, 1998, **37**, 5362-5371.

5 D. Lewis, *Biochem. J*, 1951, **49**, 149.

6 P. Gross and R. P. Smith, *CRC Crit. Rev. Toxicol.*, 1985, **14**, 87-99.

7 M. Kumasaki, Y. Fujimoto and T. Ando, *J. Loss. Prevent. Proc.*, 2003, **16**, 507-512.

8 Y. Iwata and H. Koseki, *J. Hazard. Mater.*, 2003, **104**, 39-49.

9 K. Krishna, Y. Wang, S. R. Saraf, W. J. Rogers, J. T. Baldwin, J. P. Gupta and M. S. Mannan, *Reliab. Eng. Syst. Safe.*, 2003, **81**, 215-224.

10 R. P. Smith and W. R. Layne, *J. Pharmacol. Exp. Ther.*, 1969, **165**, 30-35.

11 T. Kolasa and W. Wardencki, *Talanta*, 1974, **21**, 845-857.

12 T. You, M. Wu and E. Wang, *Anal. Lett.*, 1997, **30**, 1025-1036.

13 M. Ebadi, *Electrochim. Acta*, 2003, **48**, 4233-4238.

14 J. Li and X. Lin, *Sens. Actuators, B-Chem.*, 2007, **126**, 527-535.

15 A. Afkhami, T. Madrakian and A. Maleki, *Anal. Sci.*, 2006, **22**, 329-331.

16 F. Dias, A. S. Olojola and B. Jaselskis, *Talanta*, 1979, **26**, 47-49.

17 B. Deepa, N. Balasubramanian and K. S. Nagaraja, *Chem. Pharm. Bull.*, 2004, **52**, 1473-1475.

18 N. Teshima, S. K. M. Fernández, M. Ueda, H. Nakai and T. Sakai, *Talanta*, 2011, **84**, 1205-1208.

19 E. Kavlentis, *Microchem. J.*, 1988, **37**, 22-24.

20 P. Verma and V. Gupta, *Talanta*, 1984, **31**, 1013-1014.

21 W. Korte, *J. Chromatogr. A*, 1992, **603**, 145-150.

22 A. M. Prokai and R. K. Ravichandran, *J. Chromatogr. A*, 1994, **667**, 298-303.

23 P. N. Fernando, I. N. Egwu and M. S. Hussain, *J. Chromatogr. A*, 2002, **956**, 261-270.

24 X. Qi and R. P. Baldwin, *Electroanalysis*, 1994, **6**, 353-360.

25 Y. Seike, R. Fukumori, Y. Senga, H. Oka, K. Fujinaga and M. Okumura, *Anal. Sci.*, 2004, **20**, 139-142.

26 J. Guzowski Jr, C. Golanoski and E. Montgomery, *J. Pharm. Biomed. Anal.*, 2003, **33**, 963-974.

27 M. T. Von Breymann, M. A. De Angelis and L. I. Gordon, *Anal. Chem.*, 1982, **54**, 1209-1210.

28 J. H. Butler and L. I. Gordon, *Mar. Chem.*, 1986, **19**, 229-243.

29 R. L. Pesselman, M. J. Foral and S. H. Langer, *Anal. Chem.*, 1987, **59**, 1239-1240.

30 J. Wang, *Analytical electrochemistry*, Wiley. com, 2006.

31 A. Salimi and K. Abdi, *Talanta*, 2004, **63**, 475-483.

32 H. R. Zare, F. Chatraei and N. Nasirizadeh, *J. Braz. Chem. Soc.*, 2010, **21**, 1977-1985.

33 H. R. Zare and N. Nasirizadeh, *Electroanalysis*, 2006, **18**, 507-512.

34 H. R. Zare, Z. Sobhani and M. Mazloum-Ardakani, *Sens. Actuators, B-Chem.*, 2007, **126**, 641-647.

35 M. M. Ardakani, M. Karimi, S. Mirdehghan, M. Zare and R. Mazidi, *Sens. Actuators, B-Chem.*, 2008, **132**, 52-59.

36 H. R. Zare, S. H. Hashemi and A. Benvidi, *Anal. Chim. Acta*, 2010, **668**, 182-187.

37 H. R. Zare, N. Nasirizadeh, H. Ajamain and A. Sahragard, *Mater. Sci. Eng., C*, 2011, **31**, 975-982.

38 H. R. Zare and N. Nasirizadeh, *J. Braz. Chem. Soc.*, 2012, **23**, 1070-1077.

39 D. Nematollahi, S. Dehdashtian and A. Niazi, *J. Electroanal. Chem.*, 2008, **616**, 79-86.

40 D. Nematollahi, A. Amani and E. Tammari, *J. Org. Chem.*, 2007, **72**, 3646-3651.

41 E. Laviron, *J. Electroanal. Chem.*, 1979, **101**, 19-28.

42 H. R. Zare and A. M. Habibirad, *J. Solid State Electrochem.*, 2006, **10**, 348-359.

43 A. J. Bard and L. R. Faulkner, *Electrochemical methods: fundamentals and applications*, Wiley New York, 1980.

44 S. Antoniadou, A. Jannakoudakis and E. Theodoridou, *Synth. Met.*, 1989, **30**, 295-304.

45 C. Andrieux and J. Saveant, *J. Electroanal. Chem.*, 1978, **93**, 163-168.

46 M. M. Ardakani, P. E. Karami, H. Naeimi and B. Mirjalili, *Turk J Chem*, 2008, **32**, 571-584.

47 N. Nasirizadeh, M. S. Tehrani, M. R. Shishehbore, A. Karimi and M. A. Shirgholami, *J. Phys. Theor. Chem.*, 2010.

48 D. A. Skoog, F. J. Holler and T. A. Nieman, *Principles of Instrumental Analysis, 5th ed. Harcourt Brace and Company, Philadelphia, USA*, 1998, 380-428.

49 X. Cui, L. Hong and X. Lin, *Anal. Sci.*, 2002, **18**, 543-547.

50 M. P. N. Bui, X.-H. Pham, K. N. Han, C. A. Li, E. K. Lee, H. J. Chang and G. H. Seong, *Electrochem. Commun.*, 2010, **12**, 250-253.

51 M. M. Ardakani and Z. Taleat, *Int. J. Electrochem. Sci*, 2009, **4**, 694-706.

52 M. M. Aghayizadeh, N. Nasirizadeh, S. M. Bidoki and M. E. Yazdanshenas, *Int. J. Electrochem. Sci*, 2013, **8**, 8848-8862.

53 C. Zhang, G. Wang, M. Liu, Y. Feng, Z. Zhang and B. Fang, *Electrochim. Acta*, 2010, **55**, 2835-2840.

54 P. Kannan and S. A. John, *Anal. Chim. Acta*, 2010, **663**, 158-164.

55 E. Lee, M. S. Ahmed, J.-M. You, S. K. Kim and S. Jeon, *Thin Solid Films*, 2012.

56 P. Tomčík, P. Jenčušová, M. Krajčíková, D. Bustin, A. Manová and M. Čakrt, *J. Electroanal. Chem.*, 2006, **593**, 167-171.

57 L. Shi, T. Wu, P. He, D. Li, C. Sun and J. Li, *Electroanalysis*, 2005, **17**, 2190-2194.

58 M. R. Shishehbore, H. R. Zare, D. Nematollahi and M. Saber-Tehrani, *Anal. Method*, 2011, **3**, 306-313.

59 H. Zhang and J. Zheng, *Talanta*, 2012, **93**, 67-71.

60 L. Zheng and J.-f. Song, *J. Appl. Electrochem.*, 2011, **41**, 63-70.

**Legend of Scheme, Tables and Figures**

**Scheme 1.** Proposed mechanism for the electrochemical oxidation of 3-methoxycatechol (**1**) in the presence of benzoylacetonitrile (**2**) and preparation of. 2,2'-(4,5-dihydroxy-3-methoxy-1,2-phenylene)bis(3-oxo-3-phenylpropanenitrile) (**5**), DMPP.

**Fig. 1.** Cyclic voltammograms of GCE in $H_2O$ (0.2 mol $L^{-1}$ phosphate buffer, pH 7.0)/acetonitrile (50/50 v/v) mixture containing (a) 3-methoxycatechol (**1**) (1.0 mmol $L^{-1}$) in the absence of benzoylacetonitrile (**2**), (b) first and second scans of 3-methoxycatechol (**1**) (1.0 mmol $L^{-1}$) in the presence of benzoylacetonitrile (**2**) (1.0 mmol $L^{-1}$) and (c) benzoylacetonitrile (**2**) (1.0 mmol $L^{-1}$) in the absence of **1**. Scan rate 100 mV $s^{-1}$. $T$ = 25 ± 1°C.

**Fig. 2.** Cyclic voltammetric responses of DMPP-MWCNT-GCE in a 0.1 mol $L^{-1}$ phosphate buffer solution (pH 7.0) at different potential scan rates. Numbers 1–21 correspond to the potential scan rates of 5 to 130 mV $s^{-1}$, respectively. Insets: (A) Variations of $I_p$ versus potential scan rates. (B) Variation of $E_p$ versus the logarithm of the scan rate. (C) Magnification of the same plot of (B) for high scan rates.

**Fig. 3.** SEM images of (A) bare GCE, (B) MWCNT-GCE and (C) DMPP-MWCNT-GCE.

**Fig. 4.** Cyclic voltammograms of DMPP-MWCNT-GCE in different buffered pHs at a potential scan rate of 50 mV $s^{-1}$. Numbers 1–11 correspond to pHs of 2.0-12.0 respectively. Inset shows the variation of the conditional formal potential, $E^{0'}$, versus pH.

**Fig. 5.** Cyclic voltammograms of a bare GCE in a 0.1 mol $L^{-1}$ phosphate buffer solution (pH 7.0) in (a) the absence and (b) in the presence of 1.0 mmol $L^{-1}$ hydroxylamine. (c) as (b) at the MWCNT-GCE surface. Cyclic voltammograms of (d) DMPP-GCE and (e) DMPP-MWCNT-

GCE in a 0.1 mol $L^{-1}$ phosphate buffer solution (pH 7.0). (f) as (d) and (g) as (e) in the presence of 1.0 mmol $L^{-1}$ hydroxylamine. Potential scan rate: 50 mV $s^{-1}$. Inset: voltammograms of (d) 3-methoxycatechol (**1**) modified GCE and (e) 3-methoxycatechol (**1**) MWCNT-GCE in a 0.1 mol $L^{-1}$ phosphate buffer solution (pH 7.0). (f) as (d) and (g) as (e) in the presence of 1.0 mmol $L^{-1}$ hydroxylamine.

**Fig. 6.** Cyclic voltammograms of DMPP-MWCNT-GCE in a 0.l mol $L^{-1}$ phosphate buffer solution (pH 7.0) containing 1.0 mmol $L^{-1}$ hydroxylamine at different potential scan rates. Numbers 1–9 correspond to 2, 4, 6, 8, 10, 12, 16, 20, and 24 mV $s^{-1}$, respectively. Insets: (A) variation of the electrocatalytic peak currents, $I_p$, *vs.* the square root of potential scan rate, $v^{1/2}$, and (B), variation of the potential scan rate normalized current ($I_p\, v^{-1/2}$) *vs.* potential scan rate, *v*. (C) Tafel plots derived from the cyclic voltammograms recorded at potential scan rates of 6, 8, 12 and 16 mV $s^{-1}$.

**Fig. 7.** Chronoamperometric response at DMPP-MWCNT-GCE in a 0.1 mol $L^{-1}$ phosphate buffer solution (pH 7.0) at a potential step of 220 mV for different concentrations of hydroxylamine. Numbers of 1-7 correspond to 0.2, 0.4, 0.6, 0.8, 1.0, 1.2 and 1.4 mmol $L^{-1}$ of hydroxylamine. Insets: (A) plots of I *vs.* $t^{-1/2}$ obtained from chronoamperograms and (B) plot of the slopes of the straight lines of inset (A) *vs.* the hydroxylamine concentration.

**Fig. 8.** Differential pulse voltammograms of DMPP-MWCNT-GCE in a 0.1 mol $L^{-1}$ phosphate buffer solution (pH 7.0) containing different concentrations of hydroxylamine. Numbers 1–15 correspond to 1.0–300.0 µmol $L^{-1}$ of hydroxylamine. Insets of (A) and (B) show the plots of the electrocatalytic peak current as a function of hydroxylamine concentration for two linear ranges of 1.0–10.0 µmol $L^{-1}$ and 10.0–300.0 µmol $L^{-1}$, respectively.

**Table 1.** Comparison of electrocatalytic oxidation parameters of hydroxylamine (1.0 mmol $L^{-1}$) at the various electrode surfaces in pH 7.0.

**Table 2.** Comparison of detection limit and linear range of hydroxylamine determination at the different modified electrode surfaces.

**Table 3.** Determination and recovery results of hydroxylamine in a tap water sample at the DMPP-MWCNT-GCE surface.

**Scheme 1**

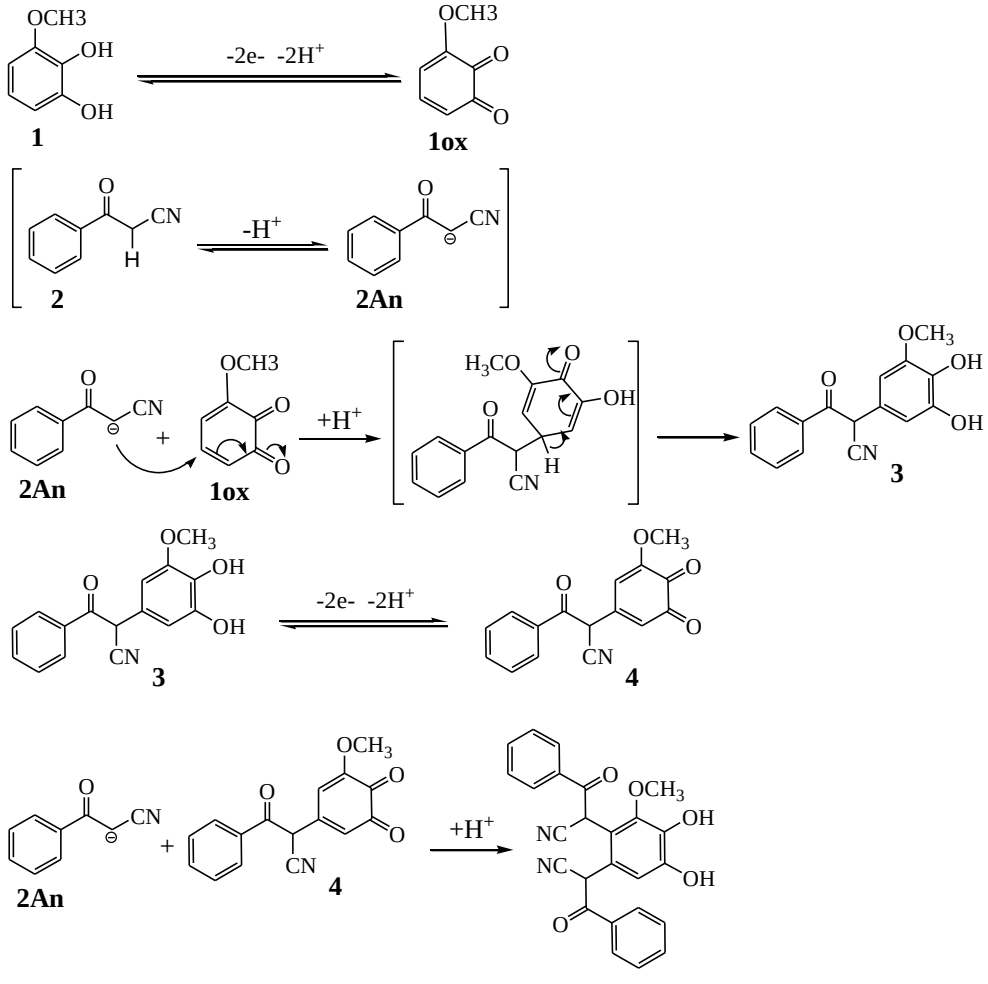


The overall reaction:

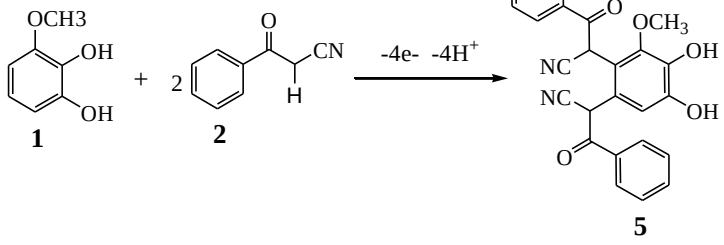

**Fig. 1.**

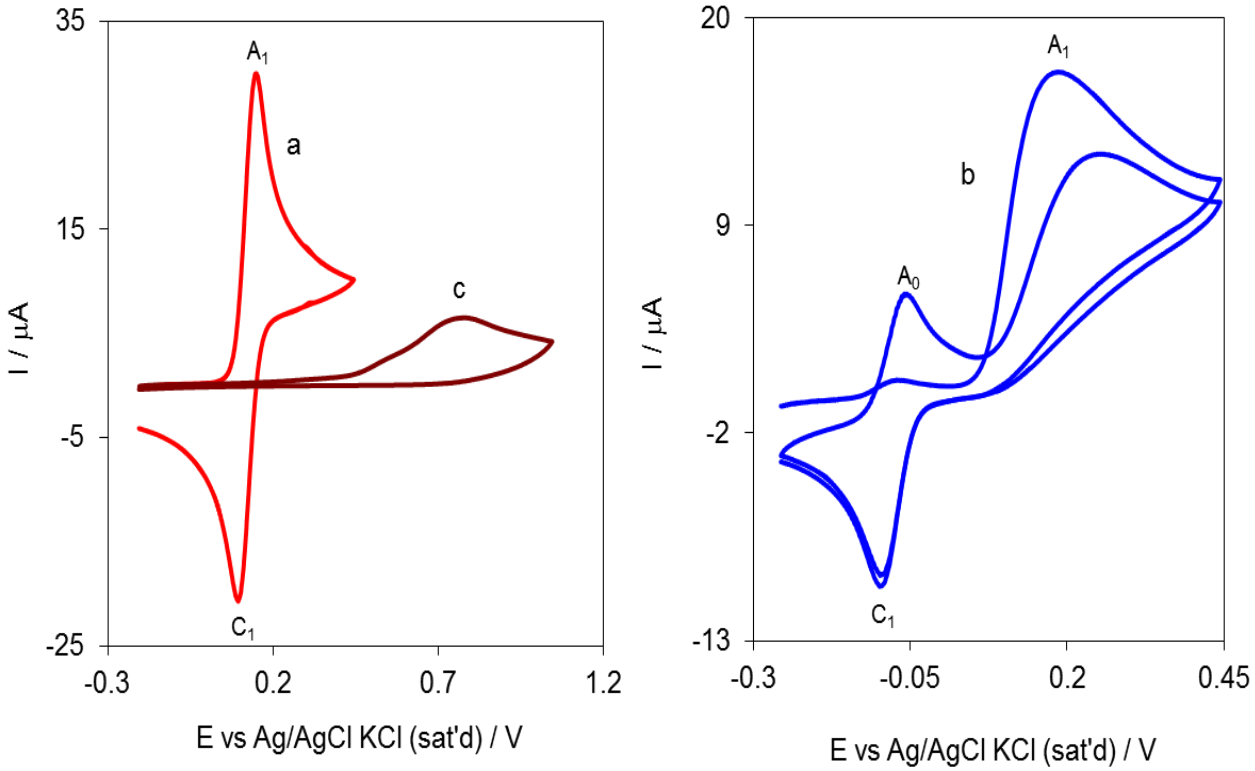

**Fig. 2.**

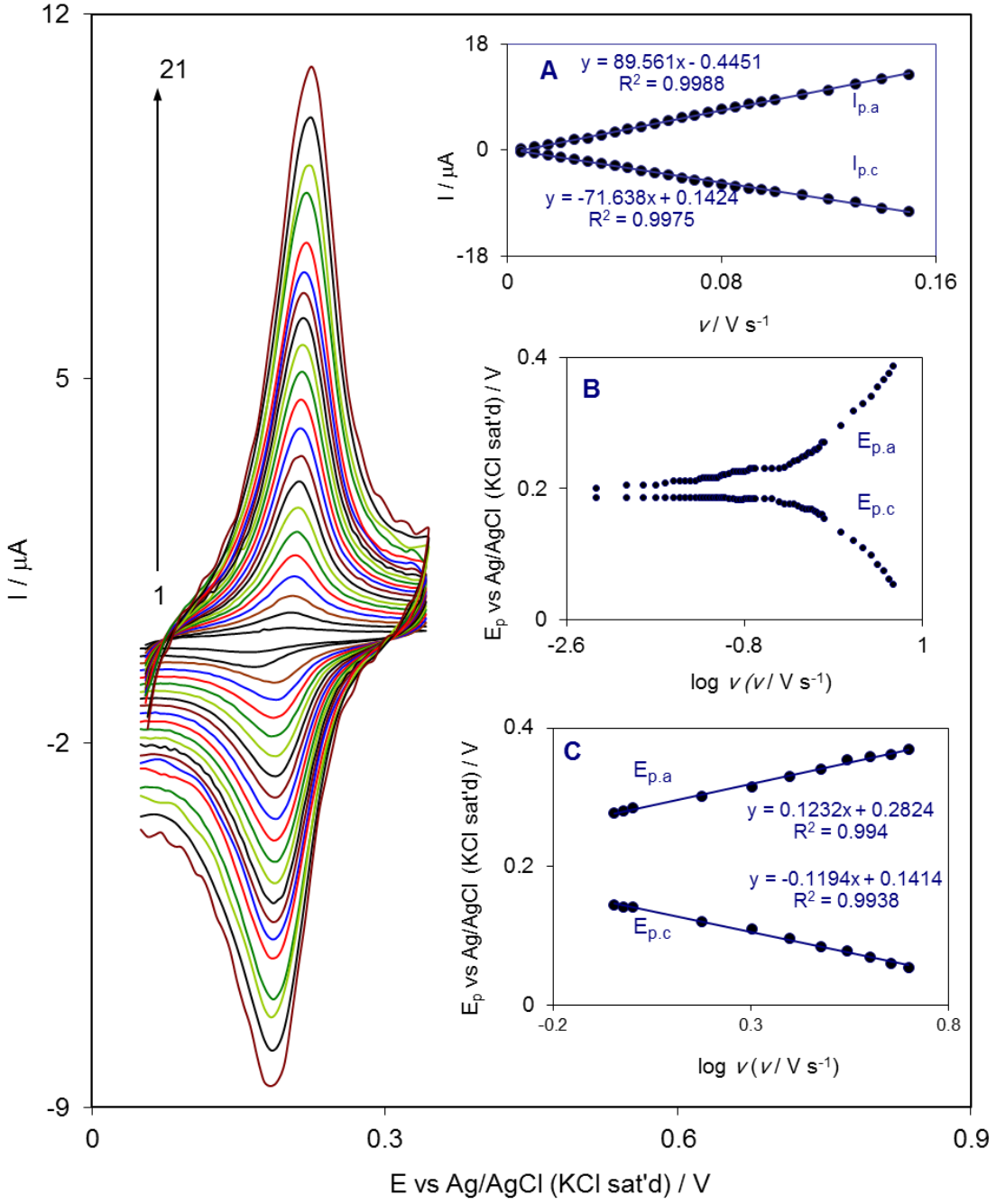

**Fig. 3.**

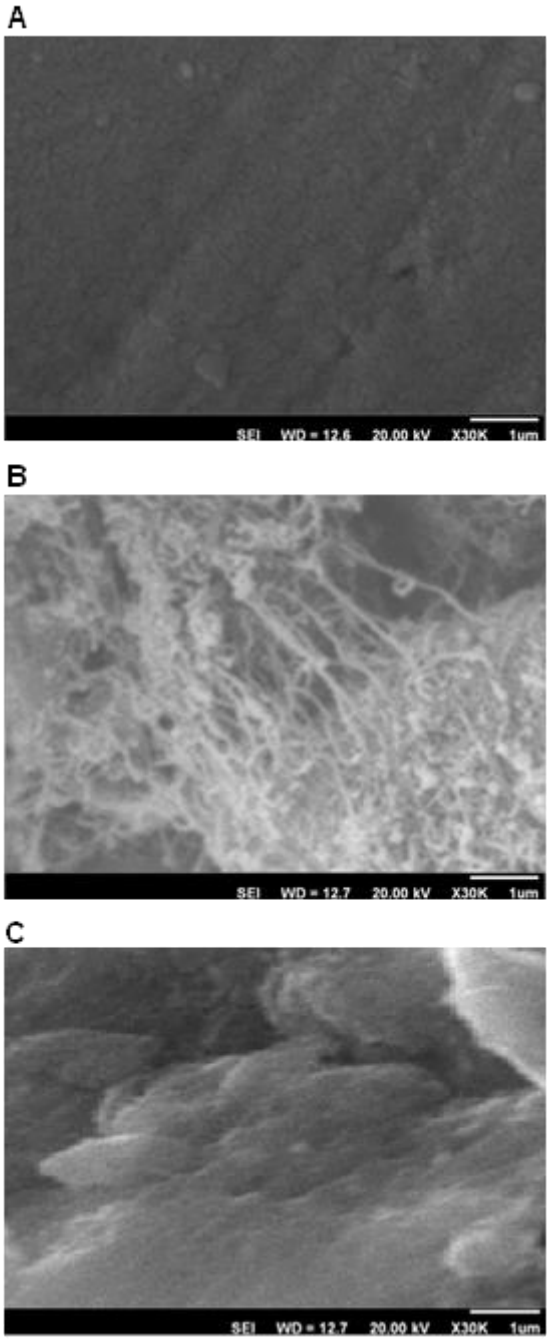

**Fig. 4.**

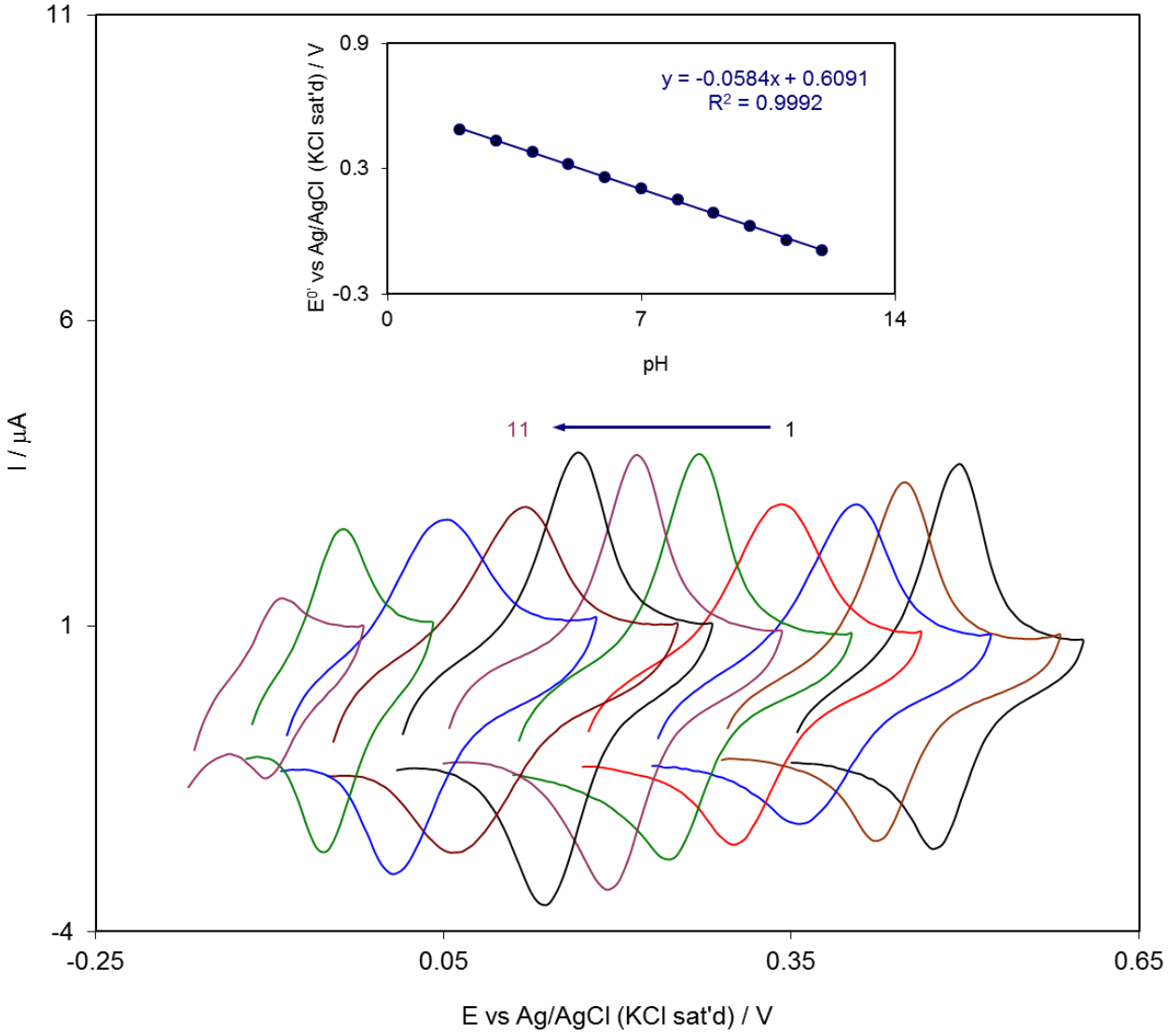

**Fig. 5.**

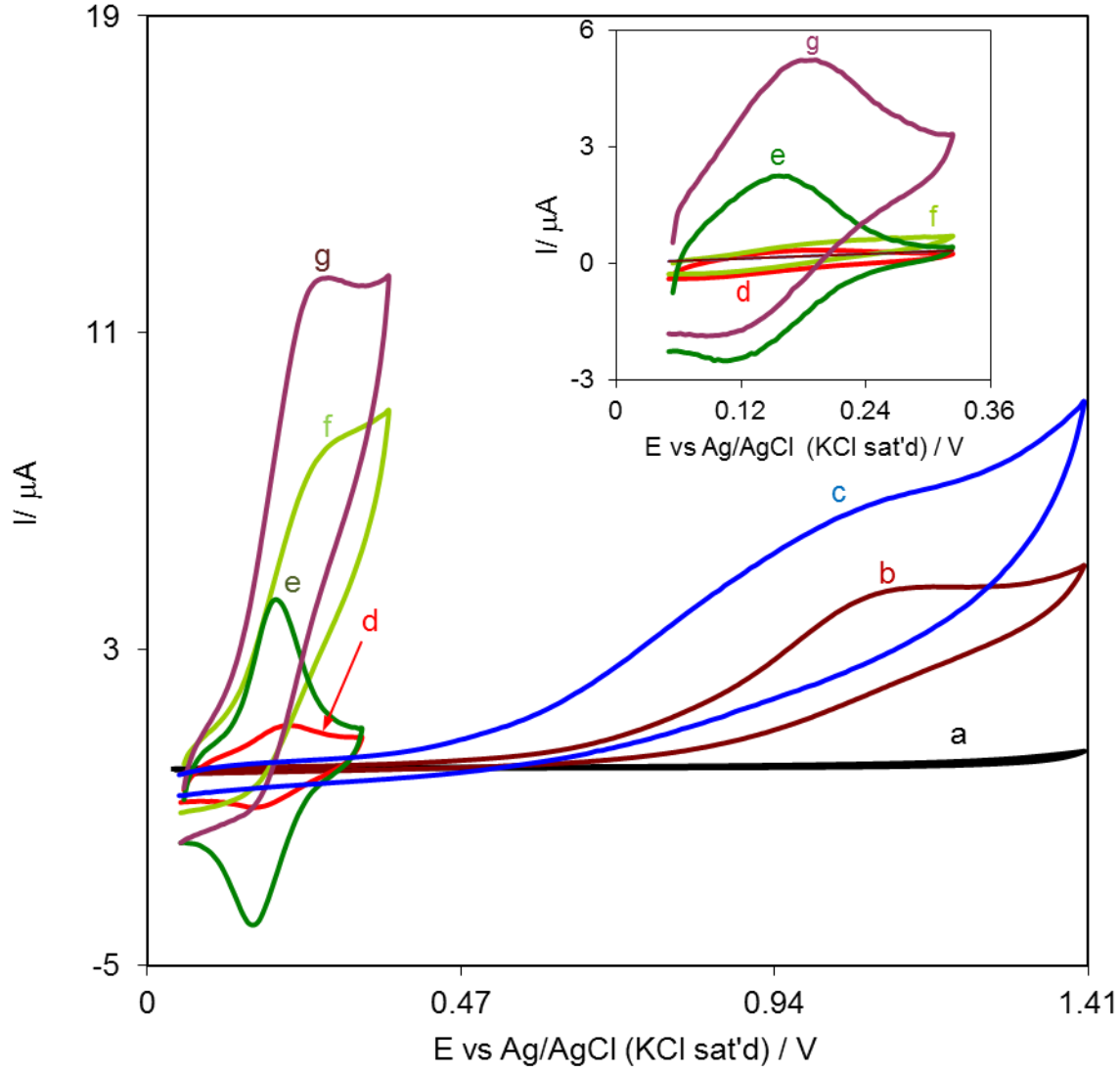

**Fig. 6**

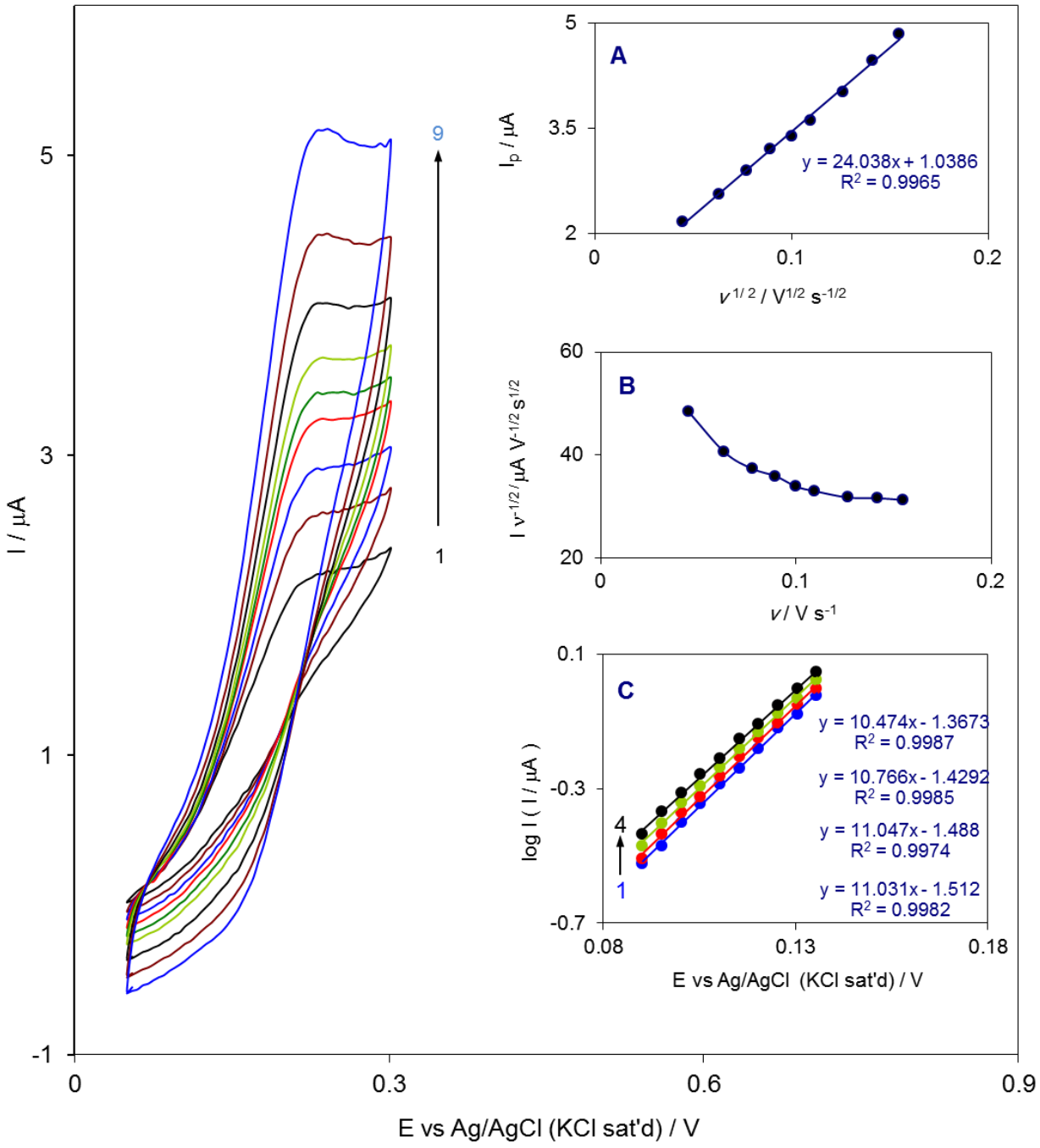

**Fig. 7**

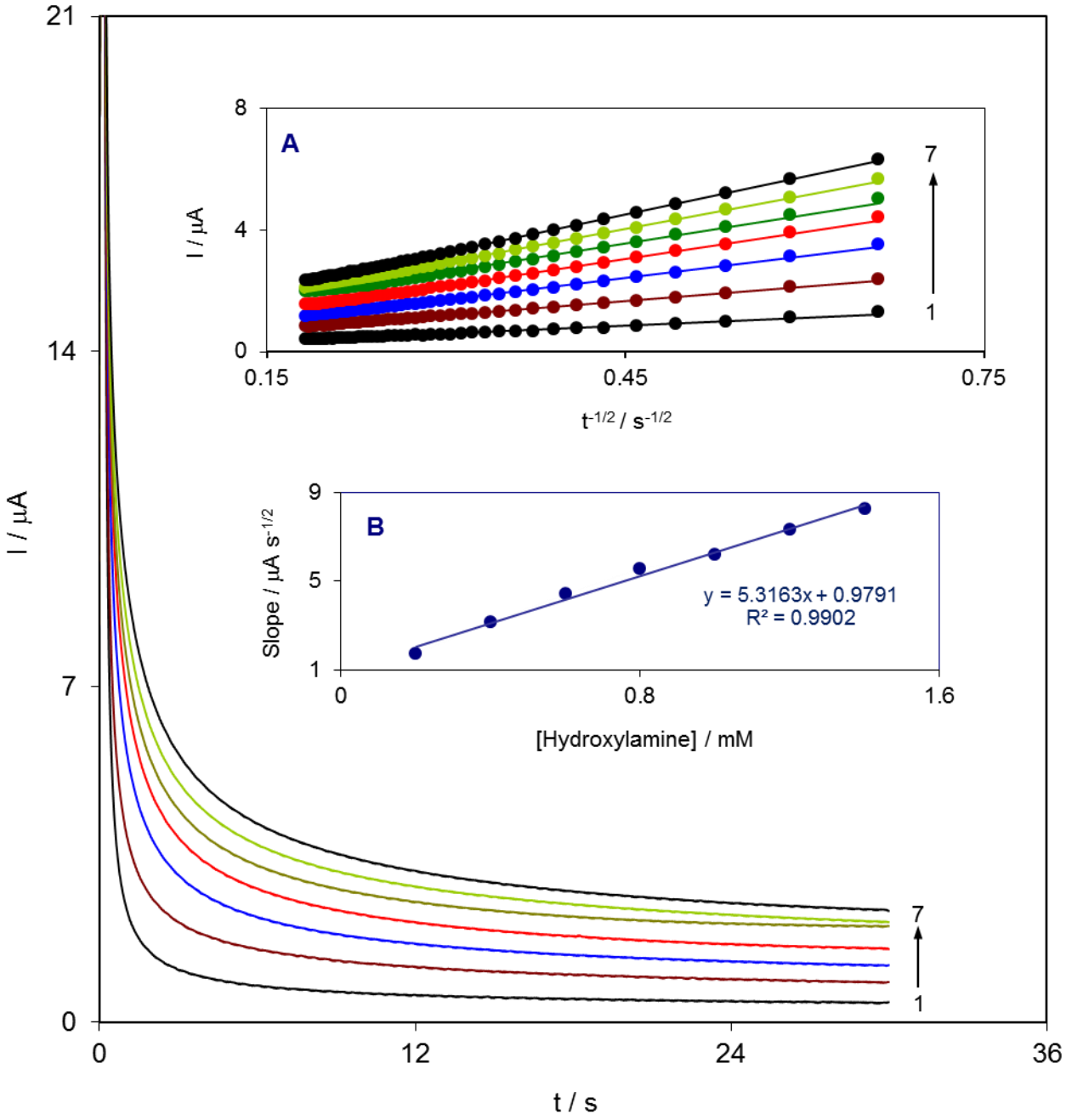

**Fig. 8**

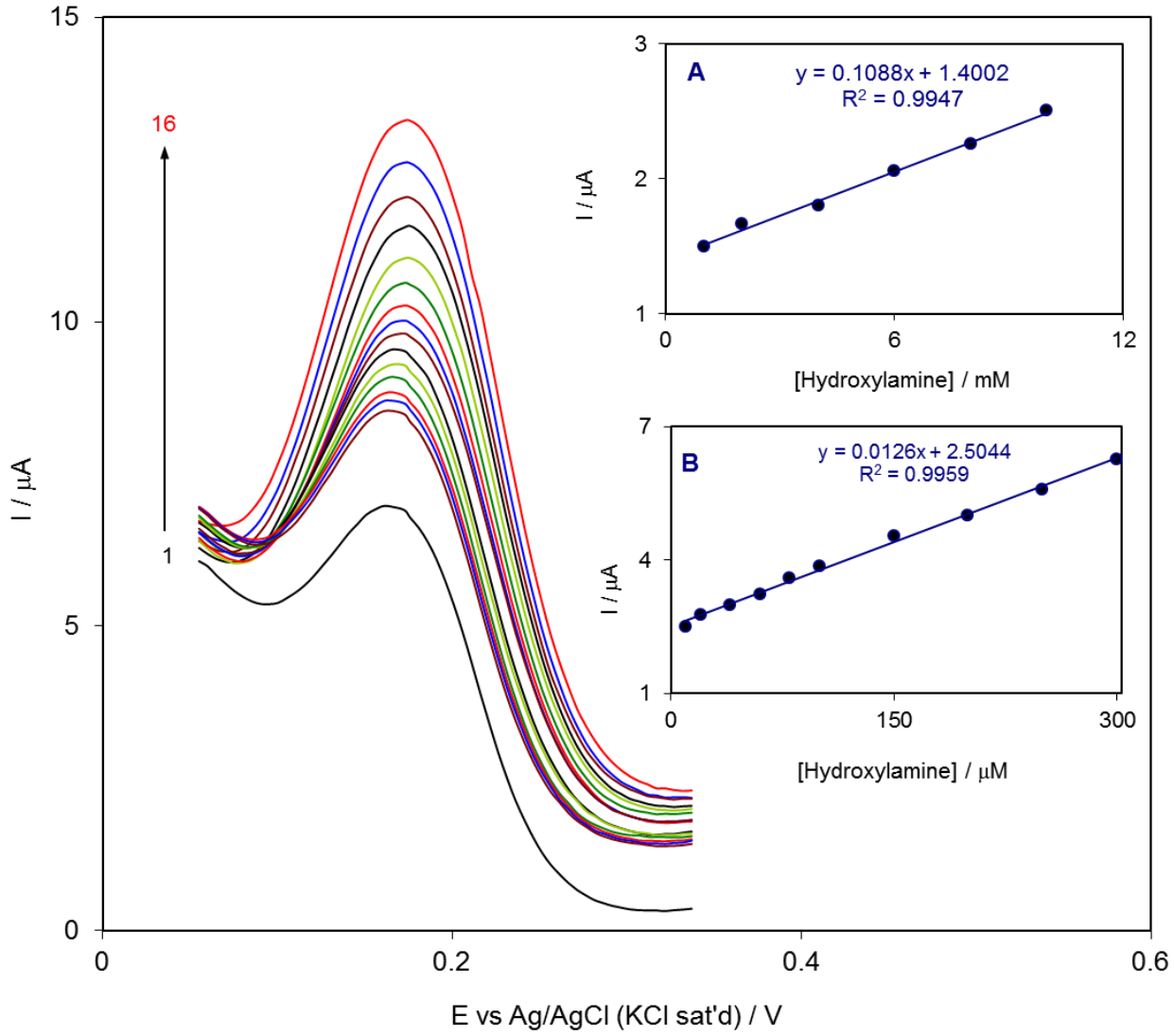

**Table 1**

| Electrode name[a] | Oxidation peak potential (mV) | Oxidation peak current (μA) |
|---|---|---|
| BGCE | 1127 | 4.5 |
| MWCNT-GCE | 1127 | 6.9 |
| DMPP-GCE | 281 | 6.1 |
| DMPP-MWCNT-GCE | 261 | 12.4 |

[a]BGCE: bare glassy carbon electrode; MWCNT-GCE: Multi-wall carbon nanotubes modified glassy carbon electrode; DMPP-GCE: 2,2'-(4,5-dihydroxy-3-methoxy-1,2-phenylene)bis(3-oxo-3-phenylpropanenitrile) modified glassy carbon electrode; DMPP-MWCNT-GCE: DMPP multi-wall carbon nanotubes modified glassy carbon electrode.

**Table 2**

| Modified electrode[a] | Linear range (μmol $L^{-1}$) | Detection limit (μmol $L^{-1}$) | Ref. |
|---|---|---|---|
| Au/PPy/GCE | 1-500; 500-18000 | 0.21 | 14 |
| NiHCF/GCE | 1.0-50.0 | 0.24 | 31 |
| IMWCNT-GCE | 1.0-10.0; 10.0-100.0 | 0.8 | 32 |
| CMCPE | 60-1000 | 10.75 | 33 |
| RMWCNT/GCE | 1.0-33.8; 33.8-81.07 | 1.0 | 34 |
| Alizarin red S/GCE | 10-800 | 7.20 | 35 |
| RuON-GCE | 4.0-33.8; 33.8-78.3 | 0.45 | 36 |
| CGA–MWCNT–GCE | 11.8-74.1; 74.1-758.6; 758.6-1939.8; 1939.8-2900.7 | 1.4 | 37 |
| OBMWCNT-GCE | 4.0-102.4; 102.4-5820.9 | 0.7 | 38 |
| OMWCNT-GCE | 2.0-600.0 | 0.61 | 47 |
| CuCoHCF/GCE | 4.6-1800.0 | 0.21 | 49 |
| AuNPs-deposited SWCNT films | 16.0-210.0 | 0.72 | 50 |
| IND-GCE | 0.5-18 | 0.16 | 51 |
| QMWCNT-GCE | 3.0-69.8; 69.8-915.2 | 0.83 | 52 |
| ZnO/MWCNTs/GCE | 0.4-19000.0 | 0.12 | 53 |
| FusedTAA-AuNPs/MPTS/Au | 0.0175-22000 | 0.00039 | 54 |
| PEDOP/MWCNTs-Pd/GCE | 1-5000 | 0.22 | 55 |
| PEDOT/MWCNTs-Pd/GCE | 1-6000 | 0.24 | |
| Titanium (IV)/Pt/ME | 10-50 | 0.20 | 56 |
| NiCoHCF/GCE | 20-200 | 0.23 | 57 |
| HTP-MWCNT-CPE | 2.0-10.0; 10.0-1000.0; 1000.0-8000.0 | 0.16 | 58 |
| BaMWCNT/GCE | 0.5-400 | 0.1 | 59 |
| Ni(II)-MR-MWCNT-PE | 2.5-400 | 0.8 | 60 |
| DMPP-MWCNT-GCE | 1.0-10.0; 10.0-300.0 | 0.37 | This work |

[a]GCE: Glassy carbon electrode; CPE: Carbon paste electrode; MWCNT: Multi-wall carbon nanotube; Au/PPy/GCE: Gold nanoparticle on pre-synthesized polypyrrole nanowire/GCE; CuCoHCF/GCE: Hybrid copper-cobalt hexacyanoferrate; NiHCF/CCE: Nickel hexacyanoferrat/carbon composite electrodes; IMWCNT-GCE: Indenedione derivative MWCNT-GCE; CMCPE: Coumestan derivative; RMWCNT/GCE: Rutin MWCNT/GCE; AuNPs-deposited SWCNT films: Gold nanoparticles single-walled carbon nanotube; RuON-GCE: Ruthenium oxide nanoparticles-GCE; CGA-MWCNT-GCE: Chlorogenic acid-MWCNT-GCE; OBMWCNT-GCE: Oracet blue MWCNT-GCE; OMWCNT-GCE: Oxadiazol derivative MWCNT-GCE; IND-GCE: Indigocarmine-GCE; QMWCNT-GCE: Thio-quinazoline derivative MWCNT-GCE; ZnO/MWCNTs/GCE: ZnO nanofilms/MWCNTs/GCE; Fused TAA-AuNPs/MPTS/Au: 2-Mercapto-4-methyl-5-thiazoleacetic acid-capped fused spherical gold nanoparticles/(3-mercaptopropyl)-trimethoxysilane/Au electrode; PEDOP/MWCNTs-Pd/GCE: Electropolymerization of 3,4-ethylenedioxypyrrole/palladium(Pd) nanoparticles/GCE; PEDOT/MWCNTs-Pd/GCE: Electropolymerization 3,4-ethylenedioxythiophene/palladium(Pd) nanoparticles/GCE Titanium (IV) on bare Pt interdigitated microelectrode; NiCoHCF/GCE: Nickel-cobalt hexacyanoferrate; HTP-MWCNT-CPE: 4-Hydroxy-2-(triphenylphosphonio)phenolate MWCNT-CPE; BaMWCNT/GCE: Baicalin MWCNT/GCE; Ni(II)-MR-MWCNT-PE: Nickel(II)-morin complex-MWCNT-paste electrode

**Table 3**

| Sample | Added (μmol $L^{-1}$) | Found[a] (μmol $L^{-1}$) | RSD (%) | Recovery % |
|---|---|---|---|---|
| Tap water | – | Not found | – | – |
| | 49.75 | 50.38±1.03 | 2.04 | 101.27 |
| | 99.01 | 101.03±1.2 | 1.19 | 102.04 |

[a]Four replicate measurements were made on the same samples, n=4.